The paper was published in the proceedings of the 11th International Conference on Physical Modelling in Geotechnics (ICPMG2026) and was edited by Ioannis Anastasopoulos. The conference was held from June 8th to June 12th 2026 in Zurich, Switzerland.

Proceedings of the 11th ICPMG 2026
11th International Conference on Physical Modelling in Geotechnics
8-12 June 2026, Zurich, Switzerland

1-g shaking table tests on a shallow-buried tunnel in liquefiable ground: deformation and displacement responses

Z. Fan
Tongji University, Shanghai, China, 2110049@tongji.edu.cn
X. Xiong
Tongji University, Shanghai, China, 2310062@tongji.edu.cn
Y. Yuan
Tongji University, Shanghai, China, yuany@tongji.edu.cn

ABSTRACT: Shallowly buried tunnels located in liquefiable soils are highly susceptible to uplift and structural damage during seismic events. To better understand this phenomenon, a 1-g shaking table test was conducted on a model tunnel embedded in liquefiable ground. A unique aspect of this study lies in the tunnel's design, which consisted of two segments differing only in surface roughness, which enables a direct evaluation of the influence of soil-structure interface friction on seismic response. The test results reveal that the presence of the tunnel substantially modified the strain development within the surrounding soil due to strong soil-structure interactions. Peak shear strains were markedly higher in the soil adjacent to the tunnel, particularly near the smooth segment. Moreover, the smooth-surfaced tunnel segment exhibited significantly greater uplift displacement than the rough-surfaced segment, confirming that surface roughness plays a critical role in controlling liquefaction-induced structural uplift. The study also found that uplift behavior of tunnels varied with seismic amplitude: under excitations with limited amplitude and duration, uplift only occurred during excitation, whereas under strong and longer excitations, secondary uplift happened after shaking ceased due to prolonged excess pore pressure dissipation and sustained upward water migration. Overall, the findings highlight the pronounced near-structure soil deformation induced by soil-structure interaction and underscore the challenges faced by numerical models in accurately simulating localized, large-strain behaviours at the tunnel-soil interface during seismic liquefaction.

1 INTRODUCTION

Soil liquefaction is one of the most destructive natural hazards in human history, often resulting in severe infrastructure damage and loss of life (Hamada et al., 1996). It typically occurs in medium-loose to loose sandy deposits that are susceptible to a loss of bearing capacity as excess pore pressure builds up during cyclic shear loading. Since underground structures usually differ from the surrounding soil in properties such as stiffness and density, their dynamic responses become coupled and exhibit strong soil-structure interaction (SSI). During liquefaction, underground structures can undergo significant displacements and deformations, leading to notable variations in both deformation and pore pressure development in the surrounding soil compared with free-field conditions.

In the past decades, numerous studies have been carried out to investigate SSI during liquefaction. For example, Chian and Madabhushi (2012) used centrifuge shaking table tests to study the effects of burial depth and diameter on the uplift behavior of circular tunnels. Their results indicated that, when the tunnel diameter remains constant, structures with shallower burial depths are more prone to uplift; whereas when the ratio of burial depth to diameter remains constant, structures with smaller diameters exhibit a more pronounced uplift tendency. Under conditions of constant burial depth, 1-g shaking table tests conducted by Nokande et al. (2023) demonstrated that the amount of uplift increases significantly as the self-weight of the structure decreases or its diameter increases. The uplift behavior of underground structures is also closely related to the liquefaction resistance of the surrounding soil. In loose, highly liquefiable soil layers, both the total uplift displacement and the rate of excess pore water pressure buildup increase markedly (Wu et al., 2023). In addition, when the amplitude or duration of the seismic input increases, the structure tends to experience more significant uplift (Sasaki and Tamura, 2004). Other related shaking table studies are largely consistent with these conclusions, and thus are not further discussed here (Castiglia et al., 2021; J. Fan et al., 2023). Although previous studies have investigated factors such as structural type, ground layering conditions, and input motion characteristics, limited attention has been given to the role of structural surface roughness during ground liquefaction. While several element tests have demonstrated the significance of soil-structure interface characteristics (Martinez and Frost, 2017, 2018), and some researchers have incorporated these effects into numerical simulations (Alyounis and Desai, 2019; Liu et al., 2021), the influence of soil-structure interface properties has, to the best of the authors' knowledge, rarely been examined through large-scale shaking table tests.

Among the several interface properties, this study focuses on investigating the effect of interface roughness on the deformation and displacement responses of both structure and surrounding soils. In what follows, Section 2 provides a brief description of the experimental setup. The discussion of the test results is given in Section 3. The conclusions drawn from the study are presented in Section 4.

2 EXPERIMENTAL SETUP

2.1 Test facilities

The shaking table tests were conducted at the State Key Laboratory of Disaster Reduction in Civil Engineering, Tongji University. The shaking table has a payload capacity of 70 tons and dimensions of 6 m × 4 m. In order to reproduce realistic boundary conditions during the seismic excitations, a biaxial laminar shear box (biLSB) was designed and utilized in this study. Additionally, a plane-type sand pluviator and a controllable flooding system were used for the preparation of the saturated soil sample. Detailed descriptions of these specialized devices are provided in a previous publication by the authors (Z. Fan et al., 2024).

2.2 Model sand

The Fujian sand was selected and used as the test sand in this study. The mechanical and dynamic behaviours of Fujian sand have been analyzed in many past studies (Gu et al., 2022; Ye et al., 2018). In order to facilitate sample saturation, only the fraction with grain sizes larger than 0.5 mm was utilized. Table 1 lists the key parameters of this sand. The sand sample was first dry-pluviated with the pluviator, and then saturated with the flooding system at the base of the shear box. The initial relative density was 45%.

Table 1. Summary of the properties for the model sand

Properties	Values
Specific Gravity G_s (-)	2.65
Friction angle φ (°)	32.8
Maximum Density ρ_{max} (kg/m^3)	1733
Minimum Density ρ_{min} (kg/m^3)	1471
Particle size D_{50} (mm)	0.78
Permeability k (m/s)	1.5e-3

2.3 Model tunnel

A square model tunnel was chosen in this study, which was made with acrylic plates. The related properties of the tunnel are given in Table 2. The distance between the ground surface and the tunnel's roof is equal to the tunnel's side length, thus the model tunnel should be considered as a shallow-buried tunnel and expected to experience uplift displacement during soil liquefaction. It should be noted that the weight of the model tunnel was adjusted to 900 kg/m³ by adding additional steel plates inside, which made its apparent density similar to that of actual tunnels. This equivalent setting of apparent mass would make the tunnel's uplift behavior during liquefaction comparable to that of actual shallow-buried tunnels. After the installation of the steel plates, the tunnel interior was injected with polyurethane foam to prevent water seepage, which may lead to the undesirable change of tunnel weight during the tests.

Table 2. Summary of the properties for the model tunnel

Properties	Properties	Values
Geometry	Total length (mm)	2200
	Segment length (mm)	1100
	Thickness (mm)	30
	Side length (mm)	300
Material	Young's modulus (GPa)	3
	Poisson's ratio (-)	0.37
	Density (kg/m^3)	1190

As shown in Figure 1, to investigate the effect of surface roughness on soil-structure interaction, the tunnel is divided into two independent segments with different surface treatments. The surface of the left-side tunnel is covered with 24-grit sandpaper to simulate the no-slip contact condition. The average particle size of the sandpaper grains is about 0.75 mm, which is similar to the characteristic particle size of the sand used in the test (0.78 mm). Thus, the sandpaper grains can be reasonably considered as sands that are firmly attached to the structure's surface, which satisfy the no-slip definition. In comparison, the right segment of the tunnel was coated with Teflon tapes to simulate a smooth contact condition. Apart from the differences in surface roughness, all other parameters of the two tunnel segments were the same. The joint part of the segments was wrapped by a 0.2 mm thick high-density polyethylene (HDPE) geotextile membrane. Due to the very low stiffness of the geotextile, the connection between the two tunnel segments can be treated as ideally flexible. Additionally, a 100 mm gap was left between each segment's end and the shear box wall. Therefore, the displacement of each tunnel segment was unaffected by the other segment or constrained by the laminar frames.

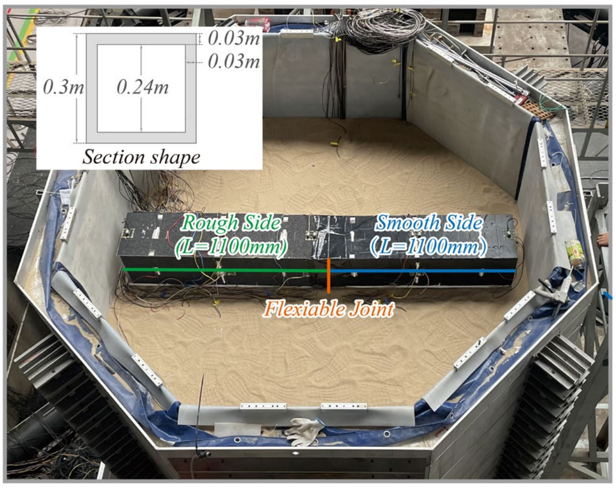

Figure 1. Illustration of the model tunnel.

2.4 Instrumentation and loading cases

Figure 2 illustrates the locations of the sensors, in which only those relevant to this study are shown. Accelerometers and piezometers were employed to measure acceleration and pore pressure responses at various locations. Sensors installed on the tunnel were affixed directly to the structural surface using a strong adhesive, while those in the field were mounted on lightweight perforated plastic plates to minimize their relative movement to the soils during excitation. Draw-wire sensors were deployed to monitor displacement responses. These used to measure ground movement were attached to perforated aluminum plates that were shallowly embedded in the ground surface, whereas those used to measure structural movement were connected to the ends of lightweight aluminum rods affixed at the denoted positions on the tunnel's top surface.

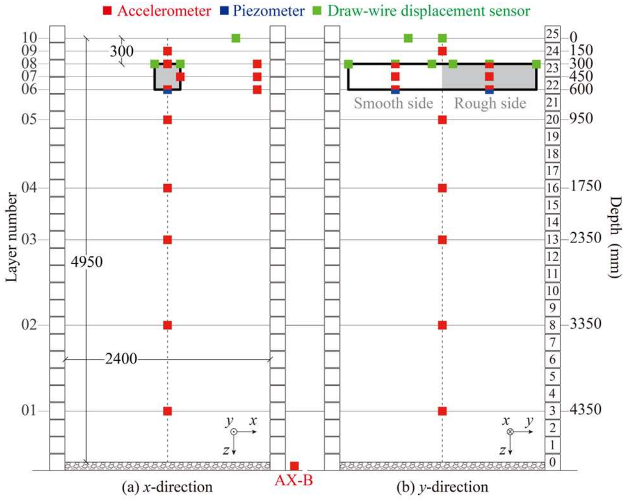

Figure 2. Location of sensors.

After the sample preparation procedure was completed, three 4-Hz sine waves were applied at the base of the shear box sequentially, with their amplitudes and number of loading cycles increasing each time. To make it easier for the shaking table to reproduce the waveform, the amplitude of the sine wave was gradually ramped up and down over the first and last five cycles. The peak base acceleration (PBA) and number of loading cycles are listed in Table 3. More information about the instrumentation and loading cases can be found in a published paper (Z. Fan et al., 2025).

Table 3. Summary of test cases

Test cases	Peak base acceleration (PBA) (g)	Number of cycles
Test-E1	0.15	20
Test-E1	0.30	20
Test-E1	0.30	40

3 TEST RESULTS AND DISCUSSION

3.1 Horizontal deformation responses

During liquefaction, saturated soil typically undergoes significant shearing and volumetric deformations, while a shallowly buried tunnel often experiences uplift displacement. In this study, ground volumetric deformation was quantified by measuring surface settlement. Both ground settlement and structural uplift were directly recorded using draw-wire sensors, whereas ground shearing deformation, i.e., shear strain, was estimated indirectly based on acceleration responses (Zeghal et al., 1995). To compare strain development at various locations, two paths were defined along the ground profile, as illustrated in Figure 3, in which Path 1 represents the far-field response and Path 2 the near-structure response.

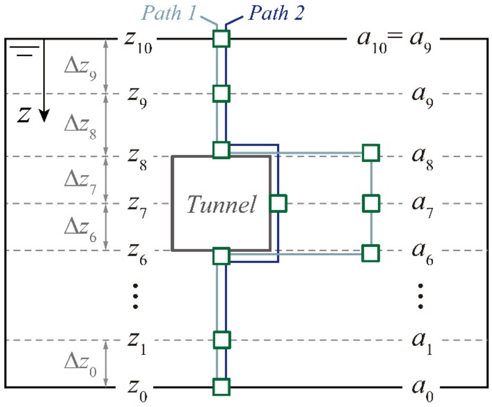

Figure 3. Locations of sensors used to calculate strain.

The evaluations of shear strain γ at the location of sensor *i* can be obtained by (Zeghal et al., 1995):

$$\gamma_i(t) = \frac{1}{\Delta z_{i-1}+\Delta z_i}\left[(u_{i-1}-u_i)\frac{\Delta z_i}{\Delta z_{i-1}} + (u_i - u_{i+1})\frac{\Delta z_{i-1}}{\Delta z_i}\right] \quad (3)$$

where u is the displacement obtained by double integration of the acceleration response, and Δz is the vertical distance between neighbouring record points.

Figure 4 presents the peak shear strain distribution along the abovementioned paths. The red curves correspond to peak strains in the far-field, while the blue and cyan curves correspond to peak strains in the near-structure zone of the rough and smooth segments of the tunnel, respectively. While comparing the peak strain distribution in the near-structure and far-field zones, it is evident that soil-structure interaction significantly altered the strain development characteristics in the region near the structure. In general, the peak strain at the bottom of the tunnel was notably higher than that at the same depth in the far-field, and also higher than the peak strains in the middle and top of the tunnel. This is consistent with the conclusion from previous studies, which show that the soil at the bottom of the tunnel is more likely to reach liquefaction during seismic loading, resulting in larger shear deformation in that region.

Regarding the effect of surface roughness, the peak strain was generally higher near the smooth side of the tunnel, except near the tunnel top during the second and third shaking events. This trend can be attributed to the lower frictional resistance along the tunnel's top and bottom surfaces on the smooth side. Because friction generally helps restrain relative movement between the tunnel and the surrounding soil, reduced friction allows greater relative displacement and, consequently, larger strains near the smooth tunnel segment.

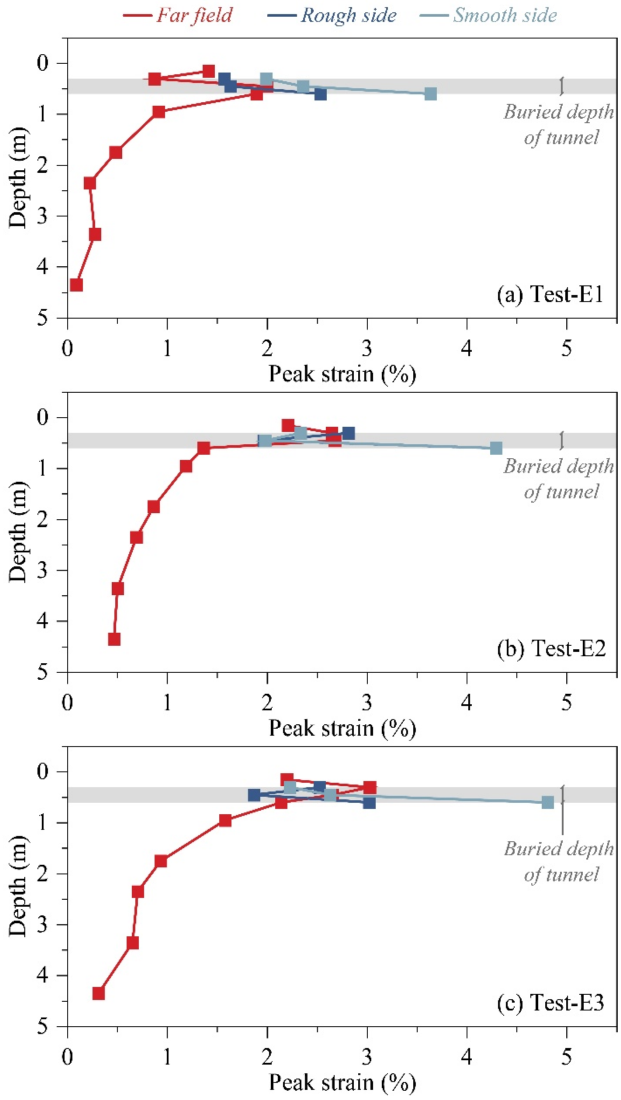

Figure 4. Comparison of peak strains in the field and near the tunnel: (a) Test-E1; (b) Test-E2; (c) Test-E3.

3.2 Vertical displacement responses

The uplifting behavior of underground structures during seismic-induced liquefaction is related to various factors such as the buried depth, cross-sectional shape, and structural density. In this study, only the effect of structural surface roughness was investigated. Figures 5-7 compared the input motion, excess pore pressure, and vertical displacement responses in each test case. In these figures, subfigure (a) presents the earthquake acceleration input at the model base, subfigure (b) compares the excess pore pressure ratio responses at the tunnel bottom and the far-field responses at the same depth, and subfigure (c) compares the vertical displacement responses for the tunnel top and ground surface. The vertical displacement of the tunnel roof is calculated as the average of the readings from two displacement sensors located at the middle of each segment, and the surface settlement is taken as the average value from the two draw-wire displacement sensors on the ground surface.

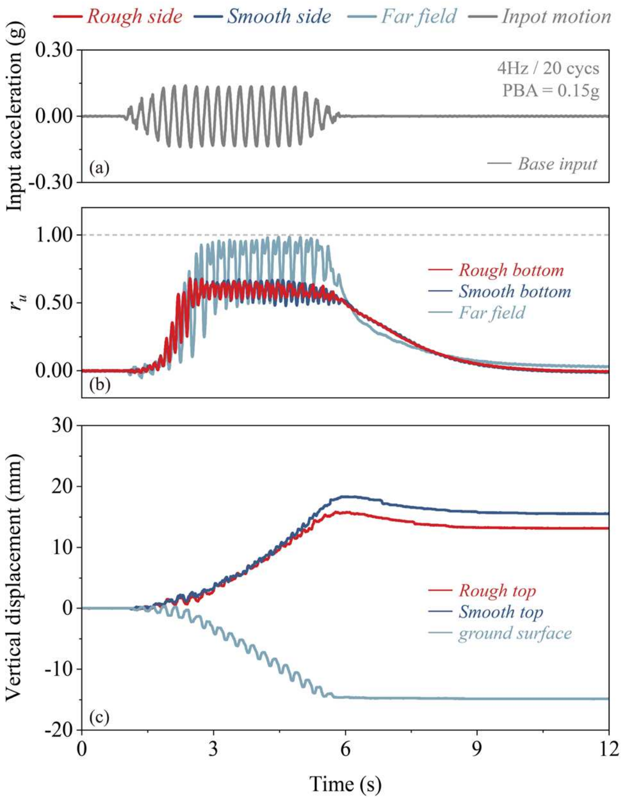

Figure 5. Measured responses in Test-E1: (a) input motion at the base; (b) excess pore pressure at the tunnel bottom and in the far field; (c) vertical displacement at the centres of the tunnel segments and at the ground surface.

Figure 5 shows the dynamic response in the test case Test-E1. In this case, only the shallower part of the ground was liquefied due to the limited input amplitude and duration. Nevertheless, Figure 5 shows that both tunnel segments experienced noticeable uplift during liquefaction. A comparison between Figures 5a and 5b reveals that as the excess pore pressure (EPP) began to accumulate in the field, the tunnel started to uplift while the ground surface simultaneously settled. When the EPP beneath the tunnel and in the far field was maintained at a stable level, the uplift rates of the two tunnel segments were initially similar. However, the uplift of the smooth segment later increased slightly and exceeded that of the rough segment. After the earthquake input ceased (as shown in Figure 5a), the excess pore pressures beneath the tunnels and in the far field began to dissipate. The ground surface continued to settle since soil consolidation was still ongoing. Both tunnel segments also moved downward along with the surrounding soil, as the uplifting forces acting on the structure during seismic excitation had diminished. It is worth noting that (Chian et al., 2014) also observed that tunnel uplift occurs solely during seismic shaking. Regarding the effect of surface roughness, Figure 5c shows that the smooth segment experienced slightly greater uplift than the rough segment, although the overall difference was not substantial.

The results in the test case Test-E2 are shown in Figure 6. Compared to Test-E1, the amplitude of the input earthquake was doubled, which results in more severe field liquefaction and structural uplift. At the beginning of the base excitation, the EPPs below the tunnel and in the far field accumulated rapidly. However, unlike what was observed in the test case Test-E1, the tunnel segments did not immediately experience uplifts at the start of the earthquake input, but instead moved downward with the surrounding soils. From Figure 6b, it is apparent that during this period, the EPP at the tunnel base and in the far-field exhibited noticeable negative peaks, indicating that the soil underwent severe dilation during cyclic shear. As a result, the initial settlement of the structure can be attributed to the soil maintaining a certain stiffness under the effect of the dilation, thereby constraining the structure and causing it to move along with the soil. As the EPP under the structure reached its peak, the EPP in the far field continues to rise slowly. At this stage, the dilation effect in the EPP response at each measurement point was no longer significant. The soil beneath the tunnel segments became fully liquefied, and the vertical displacement of the segments transitioned from settlement to uplift. While the EPP at the tunnel bottom and in the far-field reached and maintained near their peak values, the two tunnel segments rose at nearly identical rates, indicating that the surface roughness of the structure had a limited effect on their uplifting behavior. The reason is that once the surrounding soil was fully liquefied, the effective normal stress at the soil-structure interface approached zero, drastically reducing friction and thus making the effect of surface roughness on soil-structure interaction negligible.

After the input motion ceased, the EPP at the tunnel's bottom began to rapidly decrease, while the excess pore pressure ratio (EPPR) in the far field remained at 1.0. At this point, the difference in uplift displacement between the two tunnel segments increased sharply, with the smooth segment rising at a rate approximately 2.3 times that of the rough segment. This difference primarily resulted from the dissipation of EPP around the tunnel, which caused the effective stress and shear stiffness of the soil in these areas to gradually recover, which consequently enhanced the friction at the soil-structure interface. Since the magnitude of friction is positively correlated with surface roughness, the two tunnel segments exhibit significantly different uplifting behavior. Eventually, as the resisting force against uplift surpassed the driving force, both tunnel segments began to settle.

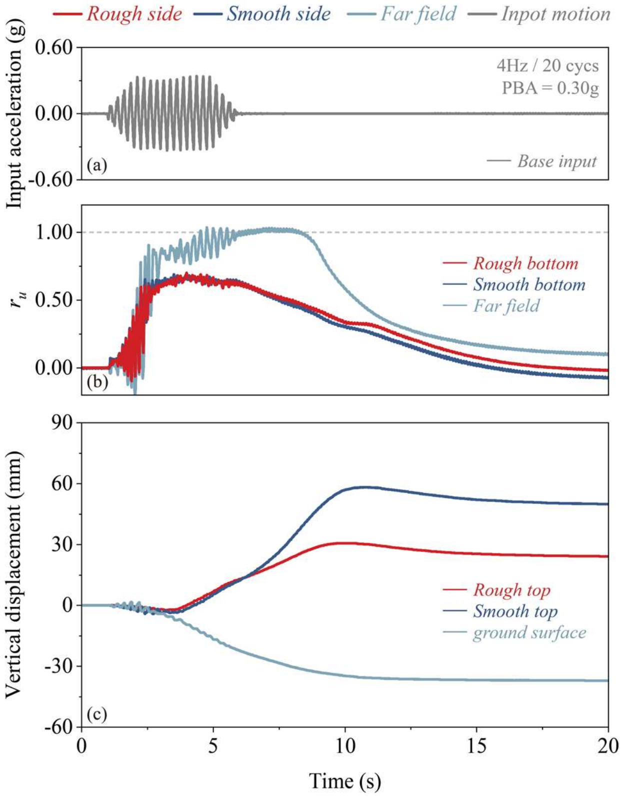

Figure 6. Measured responses in Test-E2: (a) input motion at the base; (b) excess pore pressure at the tunnel bottom and in the far field; (c) vertical displacement at the centres of the tunnel segments and at the ground surface.

Figure 7 presents the responses in the test case Test-E3. It should be noted that after the previous two seismic inputs, the two tunnel segments had already accumulated an unignorable difference in their buried depth. Consequently, the uplift rate of the smooth segment was significantly higher than that of the rough segment at the onset of excitation, due to its shallower initial burial depth and lower surface roughness. Eventually, the uplift displacement of the smooth segment exceeded the measurement range of the displacement transducer, resulting in partial data loss. Similar to the observations in Test-E2, the tunnel uplift in this test case did not cease immediately after the seismic input ended, which is different compared to the behavior observed in Test-E1. The reason for such a distinction lies in the evolution of EPP within the shallow soil layers following the earthquake. In Test-E1, the EPP in the shallow soil dissipated rapidly after the shaking stopped, whereas in Test-E2 and Test-E3, it maintained at a relatively high level. Since one of the primary driving mechanisms for structural uplift is the migration of EPP, the prolonged liquefaction in the shallow soil during Test-E2 and Test-E3 produced stronger pore water migration driven by dynamic water pressure gradients. This process resulted in a significant secondary and post-excitation uplift of the tunnels.

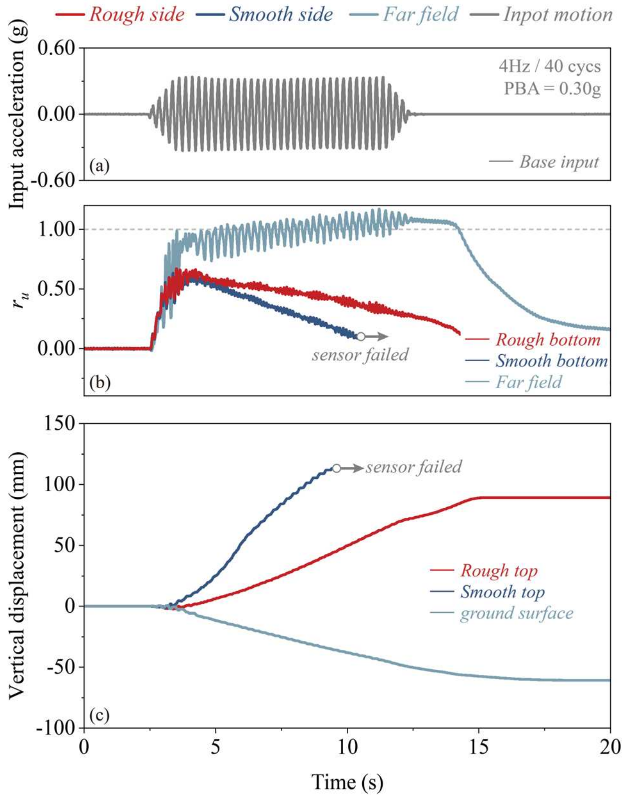

Figure 7. Measured responses in Test-E3: (a) input motion at the base; (b) excess pore pressure at the tunnel bottom and in the far field; (c) vertical displacement at the centres of the tunnel segments and at the ground surface.

4 CONCLUSION

Shallowly buried tunnels are prone to experiencing significant uplift displacement during seismic-induced liquefaction, often resulting in severe structural damage or even failure. This study conducted a 1-g shaking table test to investigate the dynamic response of a shallowly buried model tunnel located in liquefiable ground. A key distinction of the present study from previous research is that the model tunnel was divided into two segments, with only the frictional characteristics of their surfaces varied. This design enabled a direct comparison of the effects of surface roughness on soil and tunnel responses. This paper particularly examines and discusses the structural displacements, as well as the deformation responses of the surrounding soil both near and far from the structure. The main conclusions are as follows:

(1) The presence of tunnels significantly altered the development of strain in the surrounding soil due to strong soil-structure interactions. Analysis of the peak shear strain distribution indicates that the maximum shear strains at the bottoms of both tunnel segments were substantially higher than those observed in the far-field soil at the same depth. This difference can be attributed to more pronounced liquefaction in these regions due to the tunnel's unloading effect. Furthermore, during seismic excitations, the relatively low frictional resistance between the soil and the smooth surfaces at the tunnel's top and bottom surfaces allows greater relative displacement between the structure and the surrounding soil. As a result, the shear strains in the soil adjacent to the smooth tunnel segment are generally higher than those near the rough segment.

(2) It was observed that the tunnel segment with smooth surfaces exhibited significantly greater uplift than the one with rough surfaces, indicating that the surface roughness of a structure has an important and non-negligible influence on the liquefaction-induced uplift behavior of shallow-buried underground structures. In addition, the tests reveal differences in tunnel uplift behavior under different earthquake amplitudes. When the seismic amplitude was small and the field was only partially liquefied, tunnel uplift mainly occurred during seismic shaking, and the tunnel stopped uplifting and gradually began to settle after the earthquake ended. However, when the seismic amplitude was large and the ground experienced severe liquefaction, significant secondary uplift occurred even after the shaking had stopped. Since pore water migration is one of the primary mechanisms causing liquefaction-induced uplift of structures, this phenomenon can be attributed to the longer time required for the dissipation of excess pore pressure in the shallow layers of the field under strong shaking. This prolongs the pore water migration effect, thereby driving the post-seismic uplift of the structure.

In summary, this study analyses the deformation and displacement responses that occur around shallowly buried tunnels due to strong soil-structure interaction during liquefaction. It was found that the near-structural response was considerably more pronounced than the response of the surrounding soil alone. Such observation presents a significant challenge for current numerical modeling techniques, which remain limited in their ability to accurately capture large and localized deformations at the soil-structure interface during soil liquefaction.

ACKNOWLEDGEMENTS

The authors are grateful for the financial support provided by the National Natural Science Foundation of China (with grant No. 52061135112) and the Shanghai Committee of Science and Technology (with grant No. 21DZ1202803 and 22DZ1203005).

REFERENCES

Alyounis, M. E. and Desai, C. S. (2019). Testing and Modeling of Saturated Interfaces with Effect of Surface Roughness. I: Test Behavior. *International Journal of Geomechanics*, 19(8): 1–15. https://doi.org/10.1061/(asce)gm.1943-5622.0001460

Castiglia, M., Magistris, F. S., Onori, F. and Koseki, J. (2021). Response of buried pipelines to repeated shaking in liquefiable soils through model tests. *Soil Dynamics and Earthquake Engineering*, 143(December 2020): 106629. https://doi.org/10.1016/j.soildyn.2021.106629

Chian, S. C. and Madabhushi, S. (2012). Effect of buried depth and diameter on uplift of underground structures in liquefied soils. *Soil Dynamics and Earthquake Engineering*, 41: 181–190. https://doi.org/10.1016/j.soildyn.2012.05.020

Chian, S. C., Tokimatsu, K. and Madabhushi, S. P. G. (2014). Soil Liquefaction–Induced Uplift of Underground Structures: Physical and Numerical Modeling. *Journal of Geotechnical and Geoenvironmental Engineering*, 140(10): 04014057. https://doi.org/10.1061/(asce)gt.1943-5606.0001159

Fan, J., Zhao, X., Liu, J. and Huang, B. (2023). Seismic response of buried pipes in sloping medium dense sand. *Soil Dynamics and Earthquake Engineering*, 170(February): 107867. https://doi.org/10.1016/j.soildyn.2023.107867

Fan, Z., Yuan, Y., Cudmani, R., Deng, J., Chrisopoulos, S., Vogt, S. and Niebler, M. (2024). Large biaxial laminar shear box for 1-g shaking table tests on saturated sand. *Soil Dynamics and Earthquake Engineering*, 183(March): 108756. https://doi.org/10.1016/j.soildyn.2024.108756

Fan, Z., Yuan, Y., Cudmani, R., Zhang, J. and Sun, M. (2025). Experimental study on the seismic behavior of tunnels with distinct surface roughness in liquefiable soils. *Soil Dynamics and Earthquake Engineering*, 188: 109067. https://doi.org/10.1016/j.soildyn.2024.109067

Gu, X., Wu, D., Zuo, K. and Tessari, A. (2022). Centrifuge Shake Table Tests on the Liquefaction Resistance of Sand with Clayey Fines. *Journal of Geotechnical and Geoenvironmental Engineering*, 148(2). https://doi.org/10.1061/(asce)gt.1943-5606.0002708

Hamada, M., Isoyama, R. and Wakamatsu, K. (1996). Liquefaction-induced ground displacement and its related damage to lifeline facilities. *Soils and Foundations*, 36(Special): 81–97. https://doi.org/10.3208/sandf.36.special_81

Liu, W., Tian, Y. and Cassidy, M. J. (2021). An interface to numerically model undrained soil-structure interactions. *Computers and Geotechnics*, 138(July): 104327. https://doi.org/10.1016/j.compgeo.2021.104327

Martinez, A. and Frost, J. D. (2017). The influence of surface roughness form on the strength of sand-structure interfaces. *Geotechnique Letters*, 7(1): 104–111. https://doi.org/10.1680/jgele.16.00169

Martinez, A. and Frost, J. D. (2018). Undrained Behavior of Sand–Structure Interfaces Subjected to Cyclic Torsional Shearing. *Journal of Geotechnical and Geoenvironmental Engineering*, 144(9): 04018063. https://doi.org/10.1061/(asce)gt.1943-5606.0001942

Nokande, S., Jafarian, Y. and Haddad, A. (2023). Shaking table tests on the liquefaction-induced uplift displacement of circular tunnel structure. *Underground Space (China)*, 10: 182–198. https://doi.org/10.1016/j.undsp.2022.09.004

Sasaki, T. and Tamura, K. (2004). Prediction of liquefaction-induced uplift displacement of underground structures. *36th Joint Meeting US-Japan Panel on Wind and Seismic Effects*, 36: 191–198.

Wu, H., Ye, Z., Zhang, Y., Liu, H. and Liu, H. (2023). Seismic response of a shield tunnel crossing saturated sand deposits with different relative densities. *Soil Dynamics and Earthquake Engineering*, 166(January): 107790. https://doi.org/10.1016/j.soildyn.2023.107790

Ye, B., Hu, H., Bao, X. and Lu, P. (2018). Reliquefaction behavior of sand and its mesoscopic mechanism. *Soil Dynamics and Earthquake Engineering*, 114(March): 12–21. https://doi.org/10.1016/j.soildyn.2018.06.024

Zeghal, M., Elgamal, A.-W., Tang, H. T. and Stepp, J. C. (1995). Lotung downhole array. II: Evaluation of soil nonlinear properties. *Journal of Geotechnical Engineering*, 121(4): 363–378. https://doi.org/10.1061/(ASCE)0733-9410(1995)121:4(363)